Parameter Extraction for Surface Micromachined Devices Using Electrical Characterization of Sensors

M. Maute*, S. Kimmerle*, J. Franz*, J. Hauer*, D. Schubert*, H.-R. Krauss* and D. P. Kern**

*Robert Bosch GmbH, Automotive Equipment Division K8, Sensor Technology Center, Tübingerstr.123, D-72762 Reutlingen, Germany, matthias.maute@de.bosch.com
**Institute of Applied Physics, Tübingen University, Germany

ABSTRACT

This paper presents a novel methodology for the extraction of process dependent geometrical parameters of surface micromachined sensors. This approach is based on the electrical measurement of static capacitance-voltage characteristics of the sensor element on wafer level. This extraction technique is demonstrated using a surface micromachined inertial accelerometer:

a) The measurement of the capacitance-voltage characteristic (CV-characteristic) for lateral actuation of the suspended proofmass results in the extraction of a parameter related both to the thickness of the functional polysilicon layer and the lateral sidewall overetch due to the etch process of the polysilicon [1].

b) For vertical actuation of the proofmass, measurements of CV-characteristics lead to an extracted parameter that is proportional to the sidewall difference angle of the beam cross-section.

Keywords: accelerometer, micromachining, parameter extraction, CV-characteristic

1 INTRODUCTION

Current methodologies for the extraction of parameters which are relevant both to the characterization of the micromachining process and to the design of microelectromechanical systems are mainly based on electrical measurements of test structures [2-5]. Commonly, this measurement data is available only at specific wafer positions. As an extension of this extraction methodology, the sensor itself can be considered as „test structure“ to extract process dependent geometrical parameters of the polysilicon layer such as layer thickness, lateral structural overetch and sidewall difference angle from electrical measurements that can be performed with commercially available automatic wafer prober equipment. This results in a large density of the measurement data due to the large amount of sensor chips on a wafer. From an economical point of view, it is highly desirable to get information which helps to decide at a very early stage in the process flow if the chip fits the functional specifications which are relevant for the packaged sensor [6]. Furthermore, the physical models used for the extraction of geometrical parameters are also important for the design of the sensor elements.

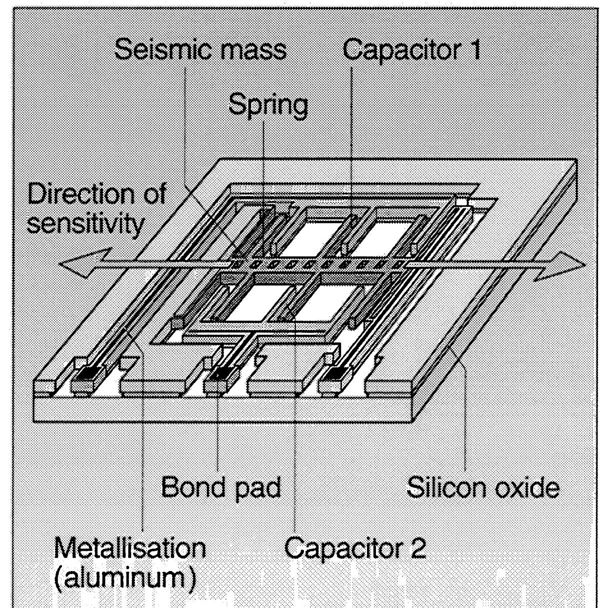

Figure 1: Principle of operation of the surface micromachined accelerometer sensor element.

We consider a surface micromachined inertial accelerometer as an example for our approach (figure 1). A polysilicon proofmass is suspended by folded tethers at each end. Upon an applied acceleration, the proofmass deflects laterally in the substrate plane. Interdigitated movable comb drives connected to the proofmass and fixed comb drives are used for differential capacitive sensing due to the dependence of the capacitance C_1 and C_2 on the applied acceleration.

2 EXPERIMENTAL SETUP

For the measurement, an HP4279A LCR meter was utilized to apply a bias voltage and to sense the capacitance with a 10mV ac signal at 120kHz. The bias voltage was applied to the fixed comb drive electrodes for lateral actuation and to the substrate for vertical actuation. The guard terminal of the LCR meter was connected to the

electrodes which were not needed for the capacitance measurement.

3 SIMULATION MODEL

3.1 Static lateral actuation

A bias voltage applied to the fixed comb drive electrodes results in a lateral displacement of the suspended proofmass due to the attractive electrostatic force. In order to capture the effects of electrostatic fringe-fields that exist above and below the comb fingers, finite-element analysis of the capacitance and the electrostatic force between the comb drive electrodes was performed. For the given sensor geometry, the length of the comb drive electrode is much larger than the gap between the electrodes and the thickness of the polysilicon layer. Therefore, the finite-element analysis was done on a cross-section model of the electrodes which includes the substrate ground plane. The numerical results from the 2-D finite-element analysis were compared to analytical expressions which are based on the model of two parallel electrode plates. The capacitance C_x and the electrostatic force F_x between movable and fixed comb drive electrodes are given by

$$C_x = \alpha_x \frac{\varepsilon N t l}{g_x - x} + \gamma_x N l \tag{1}$$

$$F_x = \beta_x \frac{\varepsilon N t l V^2}{2(g_x - x)^2} \tag{2}$$

where ε is the permittivity of the surrounding gas, g_x is the gap between the electrodes, x is the displacement of the movable comb drive electrodes, l is the length of the overlaping comb finger section, N represents the number of comb drive electrodes, t is the thickness of the polysilicon layer, V is the bias voltage across the comb electrodes, α_x and β_x are form factors that include fringe-field effects and γ_x is a parasitic capacitance per unit length that results from displacement independent fringe-fields. The fringe-field parameters were determined by fitting the analytical expressions to the finite-element simulations for various displacements up to one third of the gap since pull-in occurs for larger displacements [7]. For nominal geometrical dimensions, the capacitance fringe-field parameters were calculated as α_x = 1.12 and γ_x = 4.68pF/m. The equilibrium position can then be solved from

$$-k_x x + \beta_x \frac{\varepsilon N t l V^2}{2(g_x - x)^2} = 0 \tag{3}$$

where k_x is the spring stiffness of the beam structure. Using Eq. 1 the displacement can be eliminated and the capacitance change ΔC_x due to an applied bias voltage V can be solved from an implicit equation given by

$$\Delta C_x = \left(\frac{2k_x g_x \alpha_x^2 \varepsilon N t l}{\beta_x}\right)^{\frac{1}{3}} \left(\frac{\Delta C_x}{V^2}\right)^{\frac{1}{3}} - \alpha_x \frac{\varepsilon N t l}{g_x} \tag{4}$$

With known fringe-field form factor α_x, the process related parameter t/g_x can be obtained from a linear fit to the measured CV-characteristic. The gap g_x is given by the sum of the layout dimension and the lateral sidewall overetch as a result of the surface micromachining process. Since the capacitance change ΔC_x is measured, additional parasitic constant capacitances which are parallel to the comb drive capacitance have not to be included in the model for the CV-characteristic. Nevertheless, the parasitic capacitance can be calculated from the capacitance parameter $\alpha_x \varepsilon N t l / g_x$ which results from the linear fit and the measured capacitance without applied bias voltage.

3.2 Static vertical actuation

Applying a bias voltage to the substrate results in an attractive electrostatic force between substrate and the suspended proofmass which acts as counterelectrode. As the voltage increases, the suspended proofmass moves towards the substrate plane and the capacitance between substrate and proofmass including the comb drive electrodes increases. Assuming the same model structure given by Eq. 1 for the capacitance, the relative vertical displacement of the suspended proofmass can be calculated from the measured capacitance change ΔC_z using

$$\frac{z}{g_z} = \frac{\Delta C_z}{\Delta C_z + \alpha_z \frac{\varepsilon A_z}{g_z}} \tag{5}$$

where g_z is the gap between proofmass and the substrate plane, A_z is the overlap electrode area and α_z is a form factor due to fringe-fields. As for lateral actuation, the capacitance parameter $\alpha_z \varepsilon A_z / g_z$ can be computed from the linear fit to the measured CV-characteristic (Eq. 4).

Due to a sloped sidewall etch of the polysilicon layer, an asymmetric cross-section of the beams results from different sidewall slopes (figure 2). As a consequence, vertical actuation of the suspended proofmass also implies an additional lateral movement. The capacitances between the movable and the two adjacent fixed comb drive electrodes are given by

$$C_1 = \alpha_x \frac{\varepsilon N t}{g_x - x} + C_{p1} \tag{6}$$

$$C_2 = \alpha_x \frac{\varepsilon N t}{g_x + x} + C_{p2} \tag{7}$$

where C_{p1} and C_{p2} are parasitic constant capacitances which can be inferred from the fit to the measured lateral CV-characteristics (Eq. 4). The relative lateral displacement can then be obtained from the measured comb drive capacitances using the relation

$$\frac{x}{g_x} = \frac{C_1 - C_{p1} - C_2 + C_{p2}}{C_1 - C_{p1} + C_2 - C_{p2}} \quad (8)$$

An additional dependence of the fringe-fields form factor α_x on the vertical displacement of the comb drive electrodes does not affect the extracted relative lateral displacement.

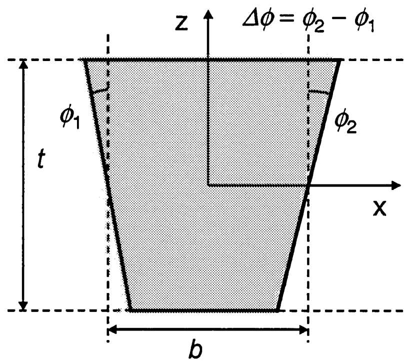

Figure 2: Cross-section geometry of the beams.

Assuming a trapezoidal beam cross-section with a small sidewall difference angle $\Delta\phi << 1$ and the same value for Young's modulus for vertical and lateral motion calculation due to isotropy of the polysilicon layer, the relative lateral displacement of the suspended proofmass for actuation towards the substrate plane is given by [8]

$$\frac{x}{g_x} = \frac{\Delta\phi}{2}\left(\frac{t}{b}\right)^2 \frac{g_z}{g_x}\frac{z}{g_z} \quad (9)$$

where b is the average width of the trapezoidal beam cross-section. Thus, the calculation of the relative lateral and relative vertical displacements from the capacitance measurements for different bias voltages applied to the substrate results in the extraction of a parameter that is proportional to the sidewall difference angle $\Delta\phi$.

4 EXPERIMENTAL RESULTS

To verify the linear dependence given by Eq. 4 for the lateral actuation, a typical measurement of the capacitance between fixed and movable comb drive electrodes due to an applied bias voltage up to the critical pull-in voltage is shown in figure 3. Plotting the capacitance change ΔC_x as a function of $\Delta C_x{}^{1/3} V^{-2/3}$ clearly results in the predicted linear dependence.

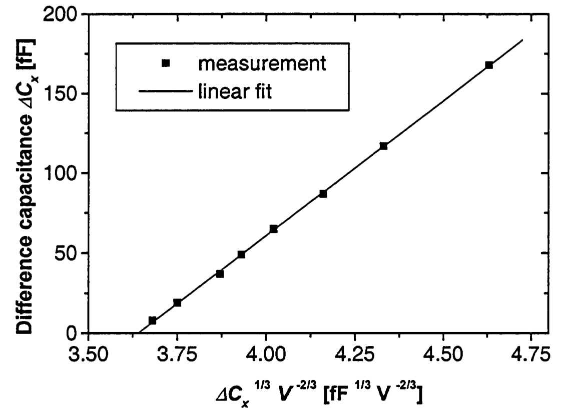

Figure 3: Typical measurement of the CV-characteristic for lateral actuation.

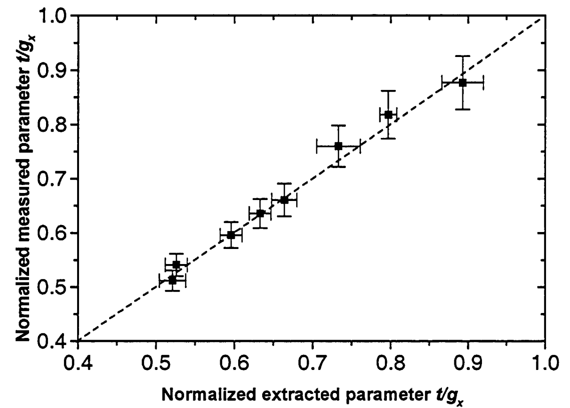

Figure 4: Normalized measured versus extracted parameter t/g_x for the lateral actuation of the proofmass.

To study the effect of the lateral sidewall overetch on the CV-characteristic, sensor elements with various gaps between fixed and movable comb drive electrodes were fabricated. To compare the electrical measurements to the simulation model, the actual thickness t of the polysilicon layer and the gap g_x were measured. For this, scanning electron micrographs (SEM) of polished cross-sections of the sensor elements were made. Due to sidewall slopes of the cross-sections resulting from the etch process of the polysilicon, an averaged gap was calculated. In figure 4, the parameters t/g_x extracted from the measured CV-characteristic using Eq. 4 versus the actual values are shown. To compensate for slightly different gaps between movable and the two opposing fixed comb drive electrodes, the CV-characteristic was measured for the lateral actuation towards both the first and the second fixed comb drive electrodes and the extracted parameters were averaged. The extracted parameters match the actual values within 4% which clearly shows that the parameter t/g_x can be obtained from the electrical measurements on wafer level.

To get information on the sidewall difference angle, the proofmass was actuated towards the substrate plane. For this, a bias voltage was applied to the substrate.

We found a dependence of the measured capacitance on the polarity of the applied bias voltage. This effect can be attributed to surface charges in dielectric surface layers [7,9]. The effect was included in the simulation model for the electrostatic force by introducing an offset voltage which accounts for the measured polarity dependence. We found offset voltages between 0.15V and 0.17V by fitting the modified physical model to the measured CV-characteristics.

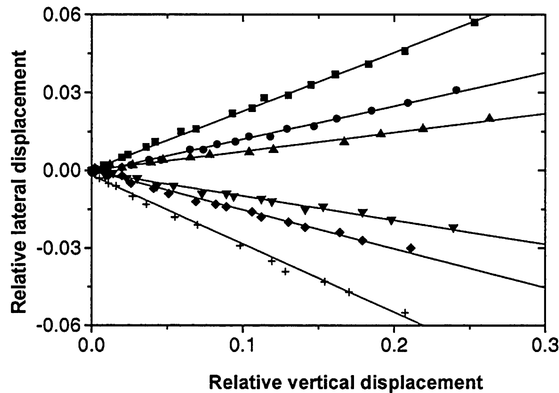

Figure 5: Relative lateral displacement versus relative vertical displacement for vertical actuation calculated from the measured capacitances.

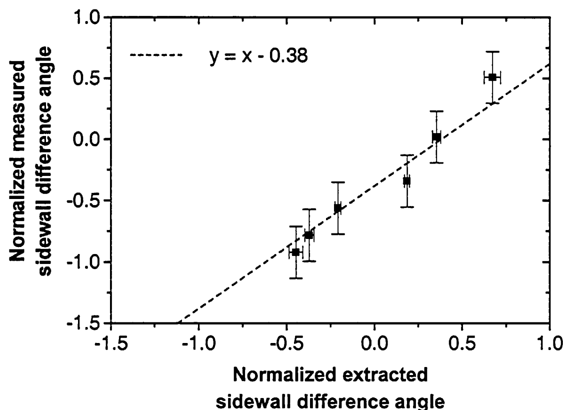

Figure 6: Normalized measured versus extracted sidewall difference angle.

Figure 5 shows measurements on six sensor elements with various sidewall difference angles for vertical actuation due to applied bias voltages to the substrate up to the critical pull-in voltage. The relative lateral displacements and the relative vertical displacements were extracted from the measured capacitances using the relations given by Eq. 5 and Eq. 8. As can be seen, the dependence is clearly linear for all six sensor elements. Employing Eq. 9, the sidewall difference angle was extracted from the measured slope. For this, the polysilicon thickness, the lateral sidewall overetch and the vertical gap were measured using micrographs of polished cross-sections. In order to verify the extracted values, the actual sidewall difference angles were also measured. We found sidewall difference angles for all six sensor cross-sections in the few degree range. The normalized measured versus extracted sidewall difference angles are shown in figure 6. We attribute the systematic error between extracted and measured values both to drift problems of the SEM and a cross-section plane which deviates from the plane perpendicular to the beam and electrode edges. Figure 6 demonstrates clearly that a parameter proportional to the sidewall difference angle can be extracted from the capacitance-voltage characteristics for vertical actuation of the proofmass.

CONCLUSION

A new methodology for parameter extraction for surface micromachined devices has been presented. As an example for this technique, the lateral and vertical actuation of the proofmass of an accelerometer sensor element was considered. Simplified analytical expressions for the capacitance and electrostatic force including fringe-field effects were derived using finite-element modelling. Fitting the physical model to the measured capacitance-voltage characteristics yields parameters related to the polysilicon thickness, the lateral sidewall overetch and the sidewall difference angle. The extracted parameters were verified using SEMs of polished cross-sections.

ACKNOWLEDGEMENT

The authors thank Doris Schielein and Artur Schulz for their help in the fabrication of the polished cross-sections.

REFERENCES

[1] M. Offenberg, F. Lärmer, B. Elsner, H. Münzel, and W. Riethmüller, Transducers '95, pp.589-592, 1995.

[2] R.K. Gupta, Ph.D. Thesis, Massachusetts Institute of Technology, USA, 1997.

[3] R.K. Gupta, P.M. Osterberg, and S.D. Senturia, Proc. of SPIE 1996 Conference: Microlithography and metrology in micromachining II, pp.39-45, 1996.

[4] P.M. Osterberg and S.D. Senturia, J. MEMS 6, no.2, pp.107-118, 1997.

[5] E.K. Chan, K. Garikipati, and R.W. Dutton, MSM '99, pp.194-197, 1999.

[6] J. Bay and J. Branebjerg, Eurosensors XIV, pp.573-576, 2000.

[7] E.K. Chan, K. Garikipati, and R.W. Dutton, J. MEMS 8, no.2, pp. 208-217, 1999.

[8] G. Lorenz, Ph.D. Thesis, Bremen University, 1999.

[9] J. Wibbeler, G. Pfeifer, and M. Hietschold, Sensors and Actuators A 71, pp.74-80, 1998.